The Astrophysical Journal Letters, 971:L9 (10pp), 2024 August 10 https://doi.org/10.3847/2041-8213/ad6572

Swift J1727.8–1613 Has the Largest Resolved Continuous Jet Ever Seen in an X-Ray Binary

Callan M. Wood[1], James C. A. Miller-Jones[1], Arash Bahramian[1], Steven J. Tingay[1], Steve Prabu[1], Thomas D. Russell[2], Pikky Atri[3], Francesco Carotenuto[4], Diego Altamirano[5], Sara E. Motta[6], Lucas Hyland[7], Cormac Reynolds[8], Stuart Weston[9], Rob Fender[4], Elmar Körding[10], Dipankar Maitra[11], Sera Markoff[12,13], Simone Migliari[14], David M. Russell[15], Craig L. Sarazin[16], Gregory R. Sivakoff[17], Roberto Soria[18,19,20], Alexandra J. Tetarenko[21], and Valeriu Tudose[22]

[1] International Centre for Radio Astronomy Research, Curtin University, GPO Box U1987, Perth, WA 6845, Australia; callan.wood@icrar.org
[2] INAF, Istituto di Astrofisica Spaziale e Fisica Cosmica, Via U. La Malfa 153, I-90146 Palermo, Italy
[3] ASTRON, Netherlands Institute for Radio Astronomy, Oude Hoogeveensedk 4, 7991 PD Dwingeloo, The Netherlands
[4] Astrophysics, Department of Physics, University of Oxford, Keble Road, Oxford, OX1 3RH, UK
[5] School of Physics and Astronomy, University of Southampton, University Road, Southampton, SO17 1BJ, UK
[6] INAF—Osservatorio Astronomico di Brera, Via E. Bianchi 46, I-23807 Merate, Italy
[7] Mathematics & Physics, School of Natural Sciences, University of Tasmania, Private Bag 37, Hobart, TAS 7001, Australia
[8] CSIRO Astronomy and Space Science, P.O. Box 1130, Bentley, WA 6102, Australia
[9] Space Operations New Zealand Ltd, Hargest House, PO Box 1306, Invercargill 9840, New Zealand
[10] Department of Astrophysics/IMAPP, Radboud University, P.O. Box 9010, 6500 GL Nijmegen, The Netherlands
[11] Department of Physics and Astronomy, Wheaton College, Norton, MA 02766, USA
[12] Anton Pannekoek Institute for Astronomy, University of Amsterdam, Science Park 904, 1098 XH Amsterdam, The Netherlands
[13] Gravitation and Astroparticle Physics Amsterdam Institute, University of Amsterdam, Science Park 904, 1098 XH 195 196 Amsterdam, The Netherlands
[14] Aurora Technology, Calle Principe de Vergara, 211, 1-B, E-28002 Madrid, Spain
[15] Center for Astrophysics and Space Science (CASS), New York University Abu Dhabi, P.O. Box 129188, Abu Dhabi, UAE
[16] Department of Astronomy, University of Virginia, 530 McCormick Road, Charlottesville, VA 22904-4325, USA
[17] Department of Physics, University of Alberta, CCIS 4-181, Edmonton AB, T6G 2E1, Canada
[18] INAF—Osservatorio Astrofisico di Torino, Strada Osservatorio 20, 10025 Pino Torinese, Italy
[19] College of Astronomy and Space Sciences, University of the Chinese Academy of Sciences, Beijing 100049, People's Republic of China
[20] Sydney Institute for Astronomy, School of Physics A28, The University of Sydney, Sydney, NSW 2006, Australia
[21] Department of Physics and Astronomy, University of Lethbridge, Lethbridge, AB, T1K 3M4, Canada
[22] Institute for Space Sciences, National Institute for Laser, Plasma and Radiation Physics, Atomistilor 409, PO Box MG-23, 077125 Bucharest-Magurele, Romania
Received 2024 May 19; revised 2024 June 30; accepted 2024 July 19; published 2024 August 5

Abstract

Multiwavelength polarimetry and radio observations of Swift J1727.8–1613 at the beginning of its recent 2023 outburst suggested the presence of a bright compact jet aligned in the north–south direction, which could not be confirmed without high-angular-resolution images. Using the Very Long Baseline Array and the Long Baseline Array, we imaged Swift J1727.8–1613 during the hard/hard-intermediate state, revealing a bright core and a large, two-sided, asymmetrical, resolved jet. The jet extends in the north–south direction, at a position angle of $-0.60° \pm 0.07°$ east of north. At 8.4 GHz, the entire resolved jet structure is $\sim 110(d/2.7\ \mathrm{kpc})/\sin i$ au long, with the southern approaching jet extending $\sim 80(d/2.7\ \mathrm{kpc})/\sin i$ au from the core, where d is the distance to the source and i is the inclination of the jet axis to the line of sight. These images reveal the most resolved continuous X-ray binary jet, and possibly the most physically extended continuous X-ray binary jet ever observed. Based on the brightness ratio of the approaching and receding jets, we put a lower limit on the intrinsic jet speed of $\beta \geqslant 0.27$ and an upper limit on the jet inclination of $i \leqslant 74°$. In our first observation we also detected a rapidly fading discrete jet knot 66.89 ± 0.04 mas south of the core, with a proper motion of 0.66 ± 0.05 mas hr^{-1}, which we interpret as the result of a downstream internal shock or a jet–interstellar medium interaction, as opposed to a transient relativistic jet launched at the beginning of the outburst.

Unified Astronomy Thesaurus concepts: Stellar mass black holes (1611); Radio jets (1347); Relativistic jets (1390); Very long baseline interferometry (1769); Low-mass x-ray binary stars (939); Transient sources (1851)

1. Introduction

Black hole (BH) low-mass X-ray binaries (LMXBs) are ideal systems to study the launching of relativistic jets and their connection to the processes of accretion, due to their proximity and variability on human timescales. The properties of relativistic jets are strongly coupled to the properties of the accretion inflow, which both evolve dramatically and rapidly during bright outbursts.

Typical BH LMXB outbursts begin in a rising hard state, where the radio emission is dominated by a compact, steady, partially self-absorbed, synchrotron-emitting, continuous jet (e.g., Corbel et al. 2000; Fender 2001). These hard-state jets become quenched as the source moves toward the transition into the soft state, via intermediate states, where bright, discrete transient jet ejecta are often launched (see, e.g., Fender et al. 2004, for a review of jets and X-ray binary outbursts).[23] The

[23] Throughout this Letter, we refer to these continuous jets as "hard-state jets" due to their historical association with the hard state, although they can persist into the hard-intermediate state, but never into the soft state.

hard-state jets are often called compact jets, due to their appearance as bright, compact point sources in high-angular-resolution observations. Resolved hard-state jets have only been observed in a few BH X-ray binaries: the high-mass X-ray binary Cyg X-1 (Stirling et al. 2001), and the LMXBs GRS 1915+105 (Dhawan et al. 2000; Ribó et al. 2004), MAXI J1836–194 (Russell et al. 2015), and MAXI J1820+070 (Tetarenko et al. 2021).

High-angular-resolution observations of resolved hard-state jets can provide independent probes of their fundamental jet properties, complementing other methods such as radio and infrared timing studies (e.g., Kalamkar et al. 2016; Malzac et al. 2018; Tetarenko et al. 2019, 2021), astrometry and core shift measurements (e.g., Miller-Jones et al. 2021; Prabu et al. 2023), and broadband spectral modeling and spectral break studies (e.g., Markoff et al. 2001; Corbel et al. 2002; Chaty et al. 2011; Gandhi et al. 2011; Russell et al. 2014a; Péault et al. 2019; Russell et al. 2020; Echiburú-Trujillo et al. 2024).

1.1. Swift J1727.8–1613

Swift J1727.8–1613 (hereafter J1727) was first detected on 2023 August 24 by Swift/BAT (Page et al. 2023), with follow-up X-ray observations revealing it to be a new candidate BH LMXB in the hard state at the beginning of a bright outburst (Castro-Tirado et al. 2023; Kennea & Swift Team 2023; Nakajima et al. 2023; Negoro et al. 2023a, 2023b; O'Connor et al. 2023a, 2023b). Optical observations suggested that J1727 has a BH primary with an early K-type companion star, with an orbital period of ∼7.6 hr at a distance of $d = 2.7 \pm 0.3$ kpc.

Optical and near-infrared observations of J1727 during the rising hard state at the beginning of the outburst showed that the source was reddening, possibly due to the onset of a compact hard-state jet (Baglio et al. 2023). Radio observations from the Submillimetre Array (SMA), the Karl G. Jansky Very Large Array, the enhanced Multi Element Remotely Linked Interferometer (eMERLIN), and the Allen Telescope Array (ATA) showed a bright, flat-spectrum, unresolved source (Baglio et al. 2023; Miller-Jones et al. 2023; Vrtilek et al. 2023; Williams-Baldwin et al. 2023). Polarization observations at X-ray wavelengths with the Imaging X-ray Polarimetry Explorer (IXPE), at optical wavelengths with the 60 cm Tohoku telescope, at 230 GHz with the SMA, and at 5.5 and 9 GHz with the Australian Telescope Compact Array (ATCA) revealed J1727 to be polarized across the electromagnetic spectrum, with a position angle consistent with being aligned in the north–south direction (Dovciak et al. 2023; Ingram et al. 2023; Kravtsov et al. 2023; Veledina et al. 2023; Vrtilek et al. 2023). These observations suggested that J1727 had a bright, compact, hard-state jet aligned in the north–south direction.

In this Letter, we present four very-long-baseline interferometry (VLBI) observations with the Very Long Baseline Array (VLBA) and the Long Baseline Array (LBA), which reveal the highly extended, resolved, north–south jet of J1727 during the hard/hard-intermediate state, as well as an apparently disconnected discrete jet knot downstream. In Section 2, we detail our observations, calibration, and imaging procedures, and in Section 3 we present our images and perform analysis on the jet, which we discuss in Section 4.

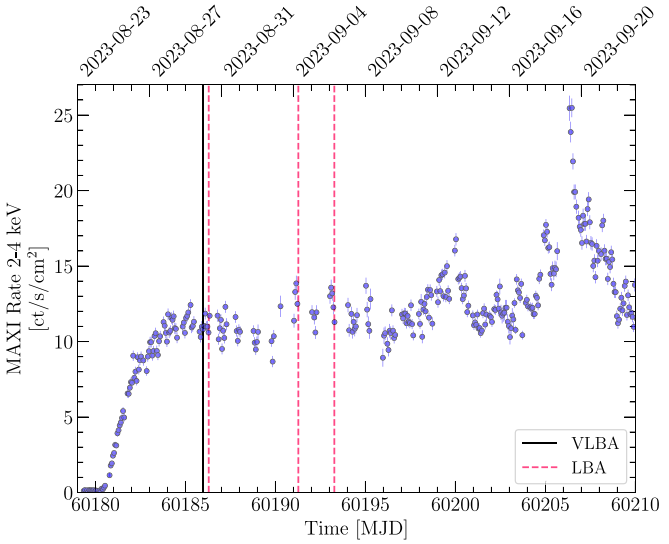

Figure 1. MAXI light curve of the evolution of Swift J1727.8–1613 at the beginning of its 2023 outburst. The times of our four VLBI observations are marked by the vertical lines, and their details are given in Table 1.

2. Observation, Calibration, and Imaging

Following the beginning of the outburst and the detection of a bright radio counterpart (Miller-Jones et al. 2023), we observed J1727 with the VLBA (project code BM538) at 8.37 GHz on 2023 August 30, as part of the Jet Acceleration and Collimation Probe Of Transient X-ray Binaries (or JACPOT XRB; Miller-Jones et al. 2011b) program. Following that observation, we observed ∼4 hr later with the LBA (project code V456) at 8.44 GHz, and then twice more on 2023 September 4 and September 6. Figure 1 shows the timing of our observations during the beginning of the outburst as seen by the Monitor of All-sky X-ray Image (MAXI; Matsuoka et al. 2009) mission.[24] The observation details can be found in Table 1. Further VLBI observations of the evolution of J1727 throughout its outburst will be presented in a future paper (C. M. Wood et al. 2024, in preparation).

For the VLBA, we used ICRF J174358.8–035004 (J1743–0350) as a fringe finder, ICRF J172134.6–162855 (J1721–1628) as a phase reference source, and ICRF J172446.9–144359 (J1724–2914) as a check source (Charlot et al. 2020). We observed geodetic blocks (Reid et al. 2009) for ∼30 minutes at the beginning and end of the observation to improve astrometric calibration. For the LBA, we used ICRF J192451.0–291430 (B1921–293; Charlot et al. 2020) as a fringe finder. In order to maximize signal-to-noise on the long baselines for phase calibration, we swapped the phase reference and check sources for the LBA. The data were correlated using the DiFX software correlator (Deller et al. 2007, 2011), and calibrated according to the standard procedures within the Astronomical Image Processing System (AIPS, version 31DEC22; Wells 1985; Greisen 2003). After the standard external gain calibration, we performed several rounds of hybrid mapping of the phase reference source to derive the time-varying phase, delay, and rate solutions, which we interpolated to J1727. We also performed a single round of amplitude self-calibration to get most accurate time-varying amplitude gain calibration, which we applied to J1727. To match the flux density scales of the VLBA and the LBA, we used the VLBA map of J1724–2914 to derive a global

[24] http://maxi.riken.jp/

Table 1
VLBI Observation Log of the Swift J1727.8–1613 Hard-state Jet

Label	Date (2023)	Time (UTC)	MJD (Midpoint)	Telescope	Observation Code	Frequency (GHz)	Bandwidth (MHz)	Stations[a]
VLBA	Aug 30	00:32:46–03:20:37	60186.08	VLBA	BM538A	8.37	512	FD, HN, KP, LA, MK, NL, OV, SC
LBA1	Aug 30	07:05:56–12:46:35	60186.41	LBA	V456H	8.44	64	CD, HB, KE, MP, PA, WW
LBA2	Sep 4	06:35:56–12:19:59	60191.39	LBA	V456I	8.44	64	AT, CD, HB, KE, MP, PA, WW
LBA3	Sep 6	06:36:02–12:19:59	60193.39	LBA	V456J	8.44	64	AT, CD, MP, PA, WW

Note.
[a] LBA stations: CD = Ceduna, HB = Hobart 12 m, KE = Katherine, MP = Mopra, PA = Parkes, WW = Warkworth 30 m, AT = ATCA.

amplitude gain solution for each LBA antenna intermediate frequency (IF) channel, and polarization to scale the a priori amplitude gains approximated from the zenith system equivalent flux densities. We used the VLBA and LBA scans of J1721–1628 to confirm that the LBA flux density scale matched the VLBA to within 5%.

We imaged J1727 within AIPS using the CLEAN algorithm (Högbom 1974) with natural weighting to maximize sensitivity, and we performed multiple rounds of phase-only self-calibration followed by a single round of amplitude self-calibration to obtain the final images.

3. Images and Analysis

Figure 2 shows the VLBA image of J1727 from 2023 August 30, which reveals a bright core with a highly resolved, asymmetric jet extending in the north–south direction, and a discrete jet knot to the south at a separation of 66.7 ± 0.2 mas from the core (which we later refined with visibility modeling). The extended continuous structure is a total of $\sim$40 mas in length, with the southern and northern jets extending $\sim$30 and $\sim$10 mas from the core, respectively.

We measured the position of the core in the VLBA image by fitting a point source to the brightest region of the jet using the AIPS task JMFIT, prior to applying any phase self-calibration. This gave a position (in the FK5 reference frame and the J2000 equinox) of

$$\begin{aligned} \text{R.A.} &= 17^{\text{h}}27^{\text{m}}43\overset{\text{s}}{.}3135784 \pm 0.0000065, \\ \text{Decl.} &= -16^{\circ}12'19.''18042 \pm 0.00033, \end{aligned}$$

where the errors are the 1σ statistical errors reported by AIPS added in quadrature with the estimated VLBA systematic astrometric errors (Pradel et al. 2006), and assuming the position of J1721–1628 to be R.A. $= 17^{\text{h}}22^{\text{m}}56\overset{\text{s}}{.}498932 \pm 0.000077$, decl. $= -16^{\circ}30'19.''26363 \pm 0.00072$.

By fitting a constant position angle to the locations of the positive flux density CLEAN components in the VLBA observations, we measured the position angle of the jet to be $-0.60^{\circ} \pm 0.07^{\circ}$ east of north. This is consistent with the position angle from the core to the southern discrete jet knot. The jet is unresolved perpendicular to the jet axis for its entire length, so based on the size of the beam and the length of the jet, we place an upper limit on the apparent jet half-opening angle of $<0.5^{\circ}$.

In Figure 3, we show all four observations of the resolved jet of J1727. These observations similarly show a bright core with an extended jet at the same position angle, however the LBA images have poorer angular resolution than the VLBA image, and thus we only resolve the southern jet. We do not see the southern discrete jet knot in any of the LBA observations. We summarize the observed peak and integrated flux densities of the observations in Table 2. The integrated flux density of the jet decreased from the first observation to the final two observations.

The LBA was slightly more sensitive to diffuse emission than the VLBA, which explains why we recovered slightly more emission at the tip of the southern jet in the first LBA observation than with the VLBA. By imaging the VLBA observation with only the shortest baselines, we were unable to detect any more diffuse emission between the extended jet and the discrete jet knot. We note that the VLBA was missing the Pie Town station, and therefore lacked a few key short baselines, which could explain why we only partially detect the diffuse emission at the tip of the southern continuous jet, causing its knotty appearance. The measured flux densities from our first two observations are consistent with the observations from eMERLIN and the ATA on 2023 August 29 and August 30, respectively (Bright et al. 2023; Williams-Baldwin et al. 2023), to within the $\sim$10% amplitude calibration uncertainties, suggesting that we have recovered most of the emission of the jet of J1727 in our observations.

For symmetric, continuous, steady-state jets inclined to the line of sight, the approaching and receding jets should be approximately symmetric, however the apparent surface brightness of these jets will be asymmetric due to relativistic aberration. The flux density ratio of approaching and receding continuous jets is given by

$$\frac{S_a}{S_r} = \left(\frac{1 + \beta \cos i}{1 - \beta \cos i}\right)^{2-\alpha}, \quad (1)$$

where S_a and S_r are the flux densities of the jets at an equal angular separation from the core, and α is the spectral index of the jets ($S_\nu \propto \nu^{\alpha}$; Ryle & Longair 1967; Scheuer & Readhead 1979; Mirabel & Rodríguez 1999). The emission from the receding jet will fall below the noise limit of an observation at a smaller separation than the approaching component, which explains the asymmetry seen in our images if the northern jet is receding and the southern jet is approaching.

Since the receding jet was only resolved in the VLBA observation, we used this observation to constrain the flux density ratio. The CLEAN components for the northern jet

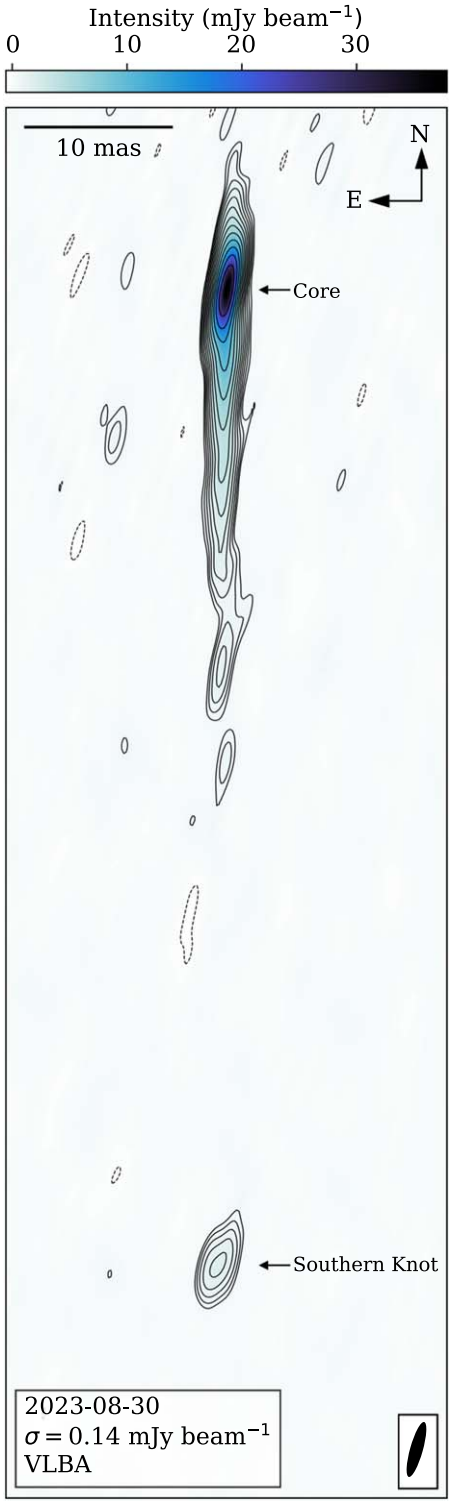

Figure 2. First VLBI image of Swift J1727.8–1613 with the VLBA. The contours mark $\pm\sigma \times \sqrt{2}^n$ mJy beam^{-1}, where $n = 3, 4, 5, \ldots$, and σ is the rms noise shown in the lower left of the image. The ellipse in the lower-right corner shows the synthesized beam. The image shows a bright core with highly resolved (∼40 mas) apparently asymmetric bipolar jets extending in the north–south direction, and a discrete jet knot to the south at a separation of 66.7 ± 0.2 mas from the core at a position angle of $179.4° \pm 0.15°$ east of north.

terminated at a separation of 6.5 mas from the core, and so we integrated the flux density of the CLEAN components along the northern and southern jets from 3 to 6.5 mas separation from the core. We chose the lower limit of 3 mas to avoid the emission of the unresolved core (see Appendix). This yielded a flux density ratio of 4.8 ± 0.4, which gave $\beta \cos i = 0.29 \pm 0.03$, assuming a spectral index of $\alpha = -0.6 \pm 0.2$ (since the extended jet should be optically thin beyond the core).

3.1. Modeling the Southern Knot

By separately imaging the first and second halves of the VLBA observation, we found that the southern knot appeared to be moving away from the core. We were able to precisely measure this motion by implementing the time-dependent model-fitting procedure described in Wood et al. (2023), where we fit a time-evolving model directly to the measured visibilities using the Bayesian inference algorithm nested sampling (Skilling 2006) implemented in the `dynesty` Python package (Speagle 2020).[25] Before modeling the knot, we subtracted the CLEAN components of the extended jet from the visibilities to create a residual observation containing only the southern knot. We then fit an analytical model directly to these residual visibilities, consisting of a circular Gaussian with fixed size moving away from the core at a fixed position angle (θ) with a constant speed ($\dot{r}$). We allowed the flux density (F) of this component to vary linearly within the observation. The flux density evolved as

$$F(t) = F_0 + \dot{F}(t - t_0), \tag{2}$$

and the position of the knot relative to the core as

$$\Delta x(t) = (r_0 + \dot{r}(t - t_0))\sin\theta \tag{3}$$

and

$$\Delta y(t) = (r_0 + \dot{r}(t - t_0))\cos\theta, \tag{4}$$

where t_0 is the reference time chosen as the approximate midpoint of the observation (02:00:00 UTC on 2023 August 30), r_0 is the separation of the jet knot from the core (in milliarcseconds) at the reference time, and Δx and Δy are in the directions of positive R.A. and decl., respectively (in milliarcseconds). We placed Gaussian priors on the separation of the jet knot at the reference time, and its position angle, based on the location of the knot in the image. We placed uniform priors on all other parameters. The prior distributions are listed in Table 3 along with the posterior estimates. We also tried models that included linear expansion of the jet knot, but found that the expansion speed was consistent with zero. Similarly, we were unable to measure any intra-observational deceleration. We also found that models with exponential or power-law flux density decays were indistinguishable from a linear decay model on the timescale of the ∼3 hr observation.

We found that the knot was clearly resolved, and was moving away from the core at a proper motion of $\dot{r} = 0.66 \pm 0.05$ mas hr^{-1}, at a position angle consistent with the extended jet position angle. We found that the jet knot was rapidly decaying over the observation, which explains why we do not see the knot in the first LBA observation ∼4 hr later. Using the separation of the knot and its ballistic speed, we calculated an ejection date of MJD 60181.8 ± 0.2, although in Section 4.4 we argue that this knot is not a discrete transient jet. The separation and FWHM size of the jet knot in the VLBA

[25] https://github.com/joshspeagle/dynesty

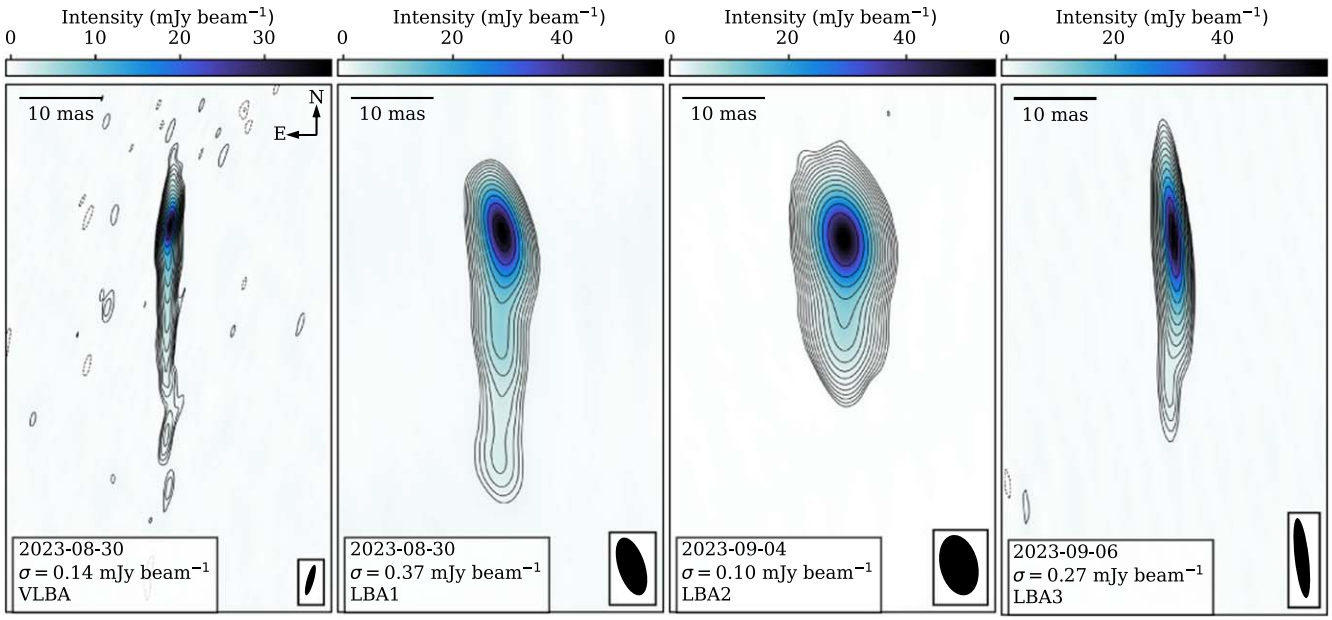

Figure 3. VLBI images of the resolved jet of Swift J1727.8–613 during the hard state. The contours mark $\pm\sigma \times \sqrt{2}^n$ mJy beam^{-1}, where $n = 3, 4, 5, \ldots$, and σ is the rms noise shown in the lower-left of each image. The ellipse in the lower-right corner of each image shows the synthesized beam. The observation parameters can be found in Table 1 and the image parameters can be found in Table 2. The jet is resolved over multiple epochs during the hard state, but appears less extended as the source moves toward the hard-intermediate state.

observation (see Table 3) give a projected half-opening angle of $0.822° \pm 0.021°$.

To ensure that the process of self-calibration was not corrupting or inducing any false variability in the data, we performed the subtraction and modeling process on versions of the observation without any self-calibration, after phase-only self-calibration, and after amplitude and phase self-calibration. We found that the position and motion of the knot was consistent between all three self-calibration scenarios, and that the size and flux density changed slightly after amplitude self-calibration. We also found marginal evidence of expansion in the observation containing amplitude self-calibration, however we only report the model parameters from the fit to the observation containing phase-only self-calibration, since we could not confirm that the amplitude self-calibration was not inducing false structure and variability in the jet knot.

4. Discussion

We have observed the highly resolved jet of Swift J1727 over four epochs with the VLBA and the LBA. The jet is continuous, extended, apparently asymmetrical, and aligned in the north–south direction. In the first observation there was also a discrete jet knot moving away from the core to the south, which does not appear in the subsequent observations. We were able to constrain the motion and flux density variability of the jet knot with time-dependent visibility model fitting.

4.1. Core Location

We measured the location of the bright core in the VLBA image, which is likely consistent with the location of the central BH. In Cyg X-1, where the base of the jet is highly free–free absorbed by the strong stellar wind of the supergiant companion (see, e.g., Miller-Jones et al. 2021), the distance between the BH and the synchrotron photosphere (where the compact "core" emission originates from) is between $\sim$1 and 3×10^{13} cm at 8.4 GHz (Zdziarski et al. 2023). Accounting for the scaling of the photosphere distance (z_0) with luminosity as $z_0 \propto L_\nu^{\sim 0.47}$ (Heinz 2006; Zdziarski et al. 2023), this would correspond to a distance of no more than 1–3 mas downstream from the location of the BH in J1727, which is within the beam of the VLBA observation projected along the jet axis. Here we have assumed that J1727 has a similar opening angle, inclination angle, and jet speed to Cyg X-1. If the inclination of the jet in J1727 is larger than the normalization in Zdziarski et al. (2023; $i = 27.5°$) then this distance will be smaller. Since J1727 contains an early K-type dwarf companion (Mata Sánchez et al. 2024), the jet is not absorbed by a strong stellar wind, and thus this is a very conservative upper limit on the distance from the BH to the jet photosphere.

We also saw no evidence of a systematic shift in the position of the core as the jet faded. We note that we had to correct for a slight offset due to the different phase calibrators for the VLBA and LBA. Subsequent observations with the VLBA later in the outburst as the extended jet contracted and transient ejecta were launched showed no significant shift in the location of the core (C. M. Wood et al. 2024, in preparation). This suggests that the distance between the photosphere and the central BH is not significant compared to the size of the restoring beam.

Any core offset in J1727 leads to an increased brightness ratio, which essentially increases the intrinsic jet speed at a given jet inclination (i.e., the brightness ratio curve constraint shifts right in Figure 5). Although we do not believe there is evidence for a significant core offset, here we report the changes for an offset of 1 mas. In such a case the estimated brightness ratio would increase to 7.1 ± 0.8, and $\beta \cos i = 0.36 \pm 0.03$, which would slightly increase the lower limit on the intrinsic jet speed and decrease the upper limit on the jet inclination (see Section 4.3). We emphasize that such a change has no strong impact on the interpretations of this Letter.

Table 2
Summary of the Jet Image Parameters from Figure 3

Observation	Integrated Flux Density (mJy)	Core Flux Density (mJy)	Beam Dimensions (mas) × (mas)	Beam Position Angle (Degrees east of north)
VLBA	101 ± 10	46 ± 5	3.9×0.9	-15.7
LBA1	90 ± 16	64 ± 6	7.3×3.3	17.7
LBA2	71 ± 8	58 ± 6	7.6×4.7	14.0
LBA3	75 ± 8	65 ± 7	9.9×1.7	6.5

Notes. The core flux density is calculated by fitting a point source to the core. Here we add a 10% amplitude calibration error in quadrature with the 1σ statistical errors reported by AIPS. The statistical error in the integrated flux density is given by $\sigma\sqrt{N_{\rm beam}}$, where σ is the rms noise in the image and $N_{\rm beam}$ is the number of independent beams in the integrated area.

Table 3
Prior Distributions and Posterior Estimates for the Moving Jet Knot in the VLBA Observation in Figure 2, Using Equations (2)–(4)

Parameter	Prior Distribution	Posterior Estimate
F_0 (mJy)	$\mathcal{U}(\min = 0, \max = 10)$	4.60 ± 0.10
$\dot{F}$ (mJy hr^{-1})	$\mathcal{U}(\min = -10, \max = 10)$	-1.11 ± 0.09
FWHM (mas)	$\mathcal{U}(\min = 0, \max = 10)$	1.92 ± 0.05
r_0 (mas)	$\mathcal{N}(\mu = 65, \sigma = 5)$	66.89 ± 0.04
$\dot{r}$ (mas hr^{-1})	$\mathcal{U}(\min = 0, \max = 10)$	0.66 ± 0.05
θ (Degrees east of north)	$\mathcal{N}(\mu = 180, \sigma = 5)$	179.24 ± 0.02

Notes. The reference time is defined as 02:00:00 (UTC) on 2023 August 30, which is approximately the midpoint of the observation. We report the median of the marginal posterior distributions as the best-fit parameters, and the 16th and 84th percentiles as the uncertainties.

4.2. Resolved Jet

The VLBA image of J1727 (Figure 2) is the most resolved image of an X-ray binary hard-state jet. Cyg X-1 and GRS 1915+105 are the only other X-ray binaries with a hard-state jet that has been resolved in an image over multiple synthesized beams (Dhawan et al. 2000; Stirling et al. 2001; Ribó et al. 2004). Assuming a distance to J1727 of 2.7 ± 0.3 kpc (Mata Sánchez et al. 2024), the size of the entire resolved jet structure (including the receding jet) was $\sim 110/\sin i$ au, and the extent of the approaching jet was $\sim 80/\sin i$ au, or $5 \times 10^8/\sin i\ r_g$ (assuming a BH mass of $8\,M_\odot$; Kreidberg et al. 2012). X-ray polarization observations of J1727 with IXPE suggested that the inclination of the inner accretion flow is between $\sim 30°$ and $60°$ (Veledina et al. 2023). Therefore, the physical extent of the approaching resolved jet of J1727 on 2023 August 30 is between ~ 95 and 160 au, or $\sim (0.6\text{–}1) \times 10^9\ r_g$.

The two-sided jets of both GRS 1915+105 and Cyg X-1 have been resolved at 8.4 GHz (Dhawan et al. 2000; Ribó et al. 2004; Miller-Jones et al. 2021). The approaching jet of Cyg X-1 has been detected out to an extent of ~ 50 au (Stirling et al. 2001; Miller-Jones et al. 2021). In 1997, the approaching jet of GRS 1915+105 was detected out to ~ 16 au (updated with the most recent distance constraint; Dhawan et al. 2000; Reid & Miller-Jones 2023), and in 2003 the jet was measured to be $\lesssim 150$ au (Ribó et al. 2004; with the upper limit due to interstellar scatter broadening). The approaching jet of MAXI J1836–194 (which has a poorly constrained distance and inclination) was marginally resolved at 8.4 GHz during the decay of its 2011 outburst, with an extent of $\sim$7–115 au (Russell et al. 2014a, 2014b, 2015). The approaching hard-state jet of MAXI J1820+070 was marginally resolved at 15 GHz, corresponding to a physical extent of ~ 3 au at 8.4 GHz (scaling the size as $z \propto 1/\nu$; Blandford & Königl 1979; Tetarenko et al. 2021).

The hard-state jet of J1727 was detected out to a further extent than the hard-state jets of Cyg X-1 and GRS 1915+105 in its 1997 flare, and MAXI J1820+070. Depending on inclination, the resolved hard-state jet of J1727 may also have been larger than the jet of GRS 1915+105 during its 2003 flare, and the decaying hard-state jet of MAXI J1836–194, and therefore J1727, may have had the most extended hard-state jet ever observed in an X-ray binary. The extent of a resolved hard-state jet is the distance from the core at which the surface brightness of the expanding jet material falls below the noise limit. This depends on both the physical properties of the jet (e.g., opening angle, jet speed, jet content, magnetic field strength, and jet internal structure), as well as the observation parameters, particularly the angular resolution, the overall sensitivity, and the sensitivity to diffuse structure.

Our measured position angle of both the extended jet and the jet knot is consistent with the radio, millimeter, and X-ray polarization position angles of J1727, which we compare in Figure 4. These measurements are also consistent with the more poorly constrained optical polarization orientation (Kravtsov et al. 2023). These measurements suggest that structures in the accretion flow, the jet base, and the downstream jet are aligned to within a few degrees in the plane of the sky.

Between the observations on 2023 August 30 and September 4 and 6, the extended continuous jet became fainter and less extended, while the core remained relatively constant. We note that the noise level in the observations changes, and thus the distance from the core to which we could detect an identical jet in each observation is different. Our LBA observations did not have sufficient angular resolution and sensitivity to resolve the counter jet, and so we cannot comment on how the jet speed changed as the compact jet faded. We cannot use the lack of a detected counter jet to place a lower limit on the brightness ratio, since the northern jet in the VLBA image can be completely contained within the beam of the subsequent LBA observations. Given the changing resolution of the observations, we also cannot meaningfully compare the peak intensity of the unresolved core across the epochs.

4.3. Intrinsic Jet Speeds

Without observing a northern counterpart to the southern jet knot, we cannot uniquely constrain the intrinsic speed and inclination of the source. However, we can constrain possible combinations of β and i. The proper motion of the approaching

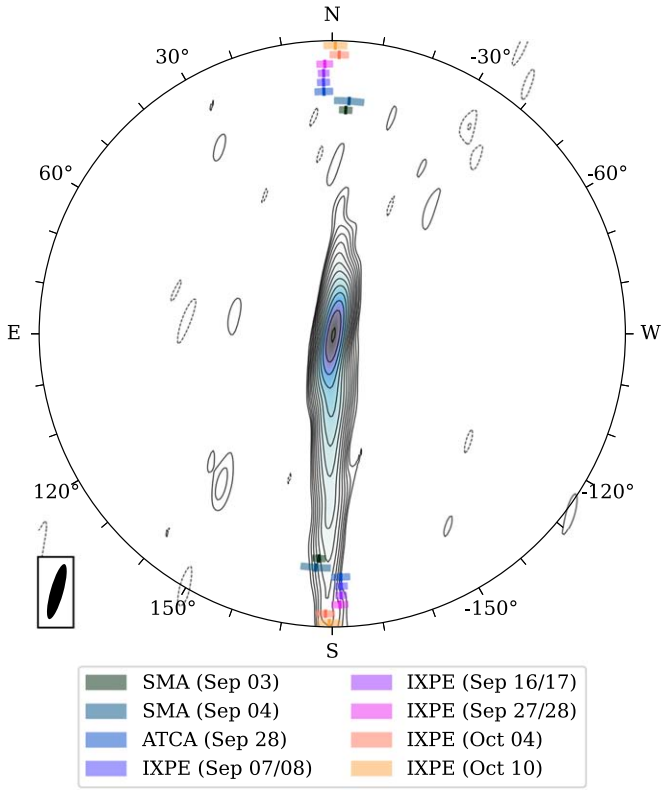

Figure 4. Comparison of polarization angles and the position angle of the resolved jet of Swift J1727.8–1613. The background image is the same as shown in Figure 2. We plot the polarization measured by the Sub-Millimeter Array at 1.3 mm (SMA; Vrtilek et al. 2023), the Australia Telescope Compact Array (ATCA) at 5.5 and 9 GHz (Ingram et al. 2023), and the Imaging X-ray Polarimetry Explorer (IXPE; Dovciak et al. 2023; Ingram et al. 2023; Veledina et al. 2023). The shaded arcs represent the reported 1σ error intervals, with the lines showing their nominal values. The polarization observations span the hard and hard-intermediate states and are consistent with the north–south orientation of the resolved jet in our VLBI observations.

jet knot, μ, is related to the intrinsic speed of the jet knot, β, by

$$\mu = \frac{\beta \sin i}{1 - \beta \cos i} \frac{c}{d}, \tag{5}$$

where i is the inclination angle of the jet to the line of sight, d is the distance to J1727(2.7 ± 0.3 kpc; Mata Sánchez et al. 2024), and c is the speed of light (Mirabel & Rodríguez 1999). We cannot use the nondetection of a receding counterpart to set an upper limit on the flux density ratio to constrain $\beta \cos i$, since we need to measure the flux densities when the jets are at equal separations (i.e., at the same age) since the jets vary in brightness as they move downstream (Miller-Jones et al. 2004).

In Figure 5, we plot the possible values of β and i for both the extended jet and the jet knot, using Equations (1) and (5), respectively. These constraints place a lower limit on the intrinsic jet speed of both the continuous and discrete jet knot of $\beta \geqslant 0.27$ and $\beta \geqslant 0.2$, respectively. The brightness ratio also gives an upper limit on the jet inclination of $i \leqslant 74°$. Although they do not have to share the same intrinsic speed, assuming that the discrete jet knot and the continuous extended jet are at the same inclination (i.e., assuming no rapid large-scale precession of the jet axis, as in V404 Cygni; Miller-Jones et al. 2019), then their intrinsic speeds are consistent within 1σ in the interval $i \sim 27°$–$37°$. In the inclination range favored by X-ray polarization measurements ($i \sim 30°$–$60°$; Veledina et al. 2023),

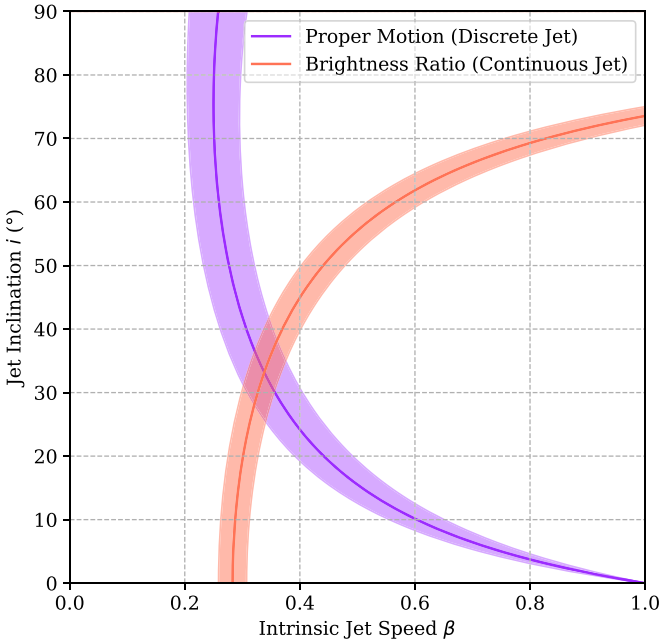

Figure 5. Constraints on the intrinsic speed and inclination of the extended and discrete jets seen in the VLBA observation in Figure 2. The solid lines show the nominal values and the shaded areas show the 1σ uncertainties. We derive these constraints from the brightness ratio of the approaching and receding arms of the extended jet (Equation (1)) and the proper motion of the southern jet knot (Equation (5)). The brightness ratio puts an upper limit on the jet inclination and a lower limit on the intrinsic speed of the continuous jet.

the jet knot is moving at the same speed or slower than the continuous jet.

4.4. Southern Jet Knot

While the nature of the jet knot is unclear, there are multiple potential scenarios. The most likely explanation is that the jet knot is the result of in situ particle acceleration in the downstream continuous jet that produced synchrotron emission. Although the approaching extended jet expanded and faded beyond detection at a separation of ~30 mas, the jet material will continue to propagate downstream until it loses its energy and momentum to the surrounding medium. An internal shock could be the result of the collision of fast-moving jet material with previously ejected slower-moving jet material. Internal shock models have been used in the past to explain both compact steady jets and discrete transient jets (Jamil et al. 2010; Malzac 2014; Malzac et al. 2018). A short-lived internal shock could explain why the jet knot was fading rapidly and was not seen in subsequent observations. This model only requires a change in the jet speed of the continuous jet as it extends outwards during the rise of the outburst. In this scenario, the jet knot does not have to be traveling at the same speed as the continuous jet.

Alternatively, the particle acceleration could be due to a collision between the continuous jet and a dense interstellar medium (ISM). The discrete knot may have then been the "leading edge" of the extended jet as it advanced outwards through the ISM. Under this scenario, and assuming ballistic motion, the continuous jet would have began extending outwards from the core on MJD 60181.8 ± 0.2, which coincides with the peak of the initial hard-state X-ray rise. If the jet knot was decelerating, then the "launch date" would have occurred later. In situ particle acceleration due to the

interaction between transient jets and the ISM has been observed to cause downstream rebrightening in multiple sources (e.g., Corbel et al. 2002, 2005; Migliori et al. 2017; Espinasse et al. 2020), as well as downstream deceleration of the jet at both arcsecond and milliarcsecond scales (e.g., Corbel et al. 2002; Yang et al. 2010; Miller-Jones et al. 2011a; Russell et al. 2019; Espinasse et al. 2020; Carotenuto et al. 2022; Bahramian et al. 2023), which may be the case here if the inclination of the jet axis is $\gtrsim 37°$. This interaction between the continuous jet and the ISM would have required a dense local environment, which can be probed by observations of the motions of transient ejecta launched later in the outburst. This explanation does not account for the rapid fading of the jet knot during the VLBA observation, as the steady continuous jet should have continued to interact with the dense ISM across all of the observations.

A less likely explanation is that knot was a discrete transient jet, which traveled ballistically away from the core after being ejected on MJD 60181.8 ± 0.2 (or later if the knot was decelerating), similar to those that are often seen in other BH LMXBs (e.g., Mirabel & Rodríguez 1994; Hjellming & Rupen 1995; Tingay et al. 1995; Miller-Jones et al. 2012; Bright et al. 2020; Carotenuto et al. 2022). These transient jets fade and become optically thin as they expand, which could explain the fading of the jet knot observed here. In other X-ray binaries, these types of jets are ejected at the peak of the outburst, during the state transition (Fender et al. 2004, 2009). In this scenario, this would be the earliest time in a BH LMXB outburst that a transient jet has been seen to have been ejected, occurring at the peak of the hard state (see Figure 1). Furthermore, these ejection events have previously been associated with specific X-ray signatures that correspond to changes in the inner accretion flow such as bright X-ray (and accompanying radio) flares, as well as a dramatic change in the X-ray spectral and timing properties (e.g., Fender et al. 2009; Miller-Jones et al. 2012; Russell et al. 2019; Homan et al. 2020; Wood et al. 2021). J1727 did exhibit many of these behaviors later in the outburst during the state transition; however, despite relatively intensive monitoring, no such clear signature of ejection was identified at the beginning of the outburst. An explanation for the jet knot that involves the reacceleration of material in the outflowing continuous jet does not require the ejection of a discrete transient jet knot during the hard/hard-intermediate state, and is more consistent with the current understanding of jet evolution during BH LMXB outbursts.

Acknowledgments

We respectfully acknowledge the significant contributions made to this longstanding collaboration by Tomaso Belloni, who sadly passed away during our observing campaign. His insights and wealth of knowledge are sorely missed by his colleagues.

The National Radio Astronomy Observatory is a facility of the National Science Foundation operated under cooperative agreement by Associated Universities, Inc. This work made use of the Swinburne University of Technology software correlator, developed as part of the Australian Major National Research Facilities Program and operated under licence. The Long Baseline Array is part of the Australia Telescope National Facility (https://ror.org/05qajvd42), which is funded by the Australian Government for operation as a National Facility managed by CSIRO. This work was supported by resources provided by the Pawsey Supercomputing Research Centre with funding from the Australian Government and the Government of Western Australia. This research has made use of the MAXI data provided by RIKEN, JAXA, and the MAXI team. This work made use of the Warkworth 30 m telescope as part of the LBA (Woodburn et al. 2015). From 2023 July 1, operation of Warkworth was transferred from Auckland University of Technology (AUT) to Space Operations New Zealand Ltd, who continue to make the facilities available for VLBI out of goodwill.

C.M.W. acknowledges financial support from the Forrest Research Foundation Scholarship, the Jean-Pierre Macquart Scholarship, and the Australian Government Research Training Program Scholarship. F.C. acknowledges support from the Royal Society through the Newton International Fellowship program (NIF/R1/211296). R.F. and S.M. acknowledge support from a European Research Council (ERC) Synergy Grant "BlackHolistic" (grant No. 101071643). D.M.R. is supported by Tamkeen under the NYU Abu Dhabi Research Institute grant CASS. A.J.T. acknowledges the support of the Natural Sciences and Engineering Research Council of Canada (NSERC; funding reference number RGPIN-2024-04458). G. R.S. is supported by NSERC Discovery Grant RGPIN-2021-0400. V.T. acknowledges support from the Romanian Ministry of Research, Innovation and Digitalization through the Romanian National Core Program LAPLAS VII-contract no. 30N/2023. The authors wish to recognize and acknowledge the very significant cultural role and reverence that the summit of Maunakea has always had within the indigenous Hawaiian community. We are most fortunate to have the opportunity to conduct observations from this mountain. We also wish to acknowledge the Gomeroi, Gamilaroi, and Wiradjuri people as the traditional custodians of the LBA observatory sites.

Facilities: MAXI, VLBA.

Software: AIPS (Wells 1985; Greisen 2003), ADS (https://ui.adsabs.harvard.edu/), Arxiv (https://astrogeo.org/), Astrogeo (https://astrogeo.org/), Astropy (Astropy Collaboration et al. 2013, 2018, 2022), CDS (Simbad; Wenger et al. 2000), Cmasher (van der Velden 2020), Corner (Foreman-Mackey 2016), Dynesty (Speagle 2020), eht-imaging (Chael et al. 2018), Jupyter (Kluyver et al. 2016), Matplotlib (Hunter 2007), Numpy (Harris et al. 2020), Scipy (Virtanen et al. 2020)

Appendix
Hard-state Jet Profile

To investigate the brightness ratio of the extended jet in Figure 2, we extracted intensity profiles down the northern and southern jets. We first rotated the image of the jet so that it aligns vertically, and then took one-dimensional cross sections of the northern and southern jets every 1.05 mas downstream from the core (7 pixels). We fit these cross sections with a one-dimensional Gaussian profile to measure the intensity of the approaching and receding jets as a function of separation from the core, which we show in Figure 6. We fitted the Gaussian profiles to the pixel intensities using nonweighted least-squares regression with `scipy.optimize.curve_fit`, where we report the intensity of the jet as the amplitude of the Gaussian profile.[26] To calculate the uncertainty in the intensity, we added in quadrature the reported 1σ statistical uncertainty from the fit (extracted from the diagonal elements of the covariance matrix), the rms noise in the image, and a 10% calibration

[26] https://docs.scipy.org/doc/scipy/reference/generated/scipy.optimize.curve_fit.html

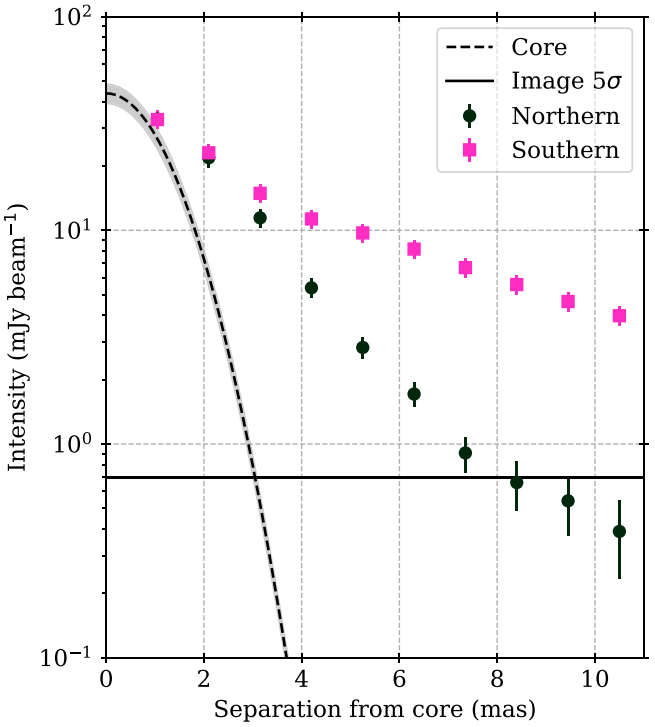

Figure 6. Intensity profile along the northern and southern jets as a function of separation from the core in the VLBA observation of Swift J1727.8–1613 shown in Figure 2. The intensity profiles are calculated by fitting one-dimensional Gaussians perpendicular to the jet axis at intervals of ∼1 mas. The dashed line shows the contribution from the core, calculated by multiplying the intensity of the core by the profile of the restoring beam along the jet axis, with the shaded region showing its uncertainty (derived from the fit).

error. In Figure 6, we also show the contribution of the unresolved core by taking the one-dimensional profile of the restoring beam along the jet axis multiplied by the fit intensity of the core. The contribution from the unresolved core drops below the 5σ limit at a separation of ∼3 mas. We note that the measurements are correlated along the jet and across the core, since the true intensity profile of the jet is convolved with the Gaussian restoring beam. This explains why the decay of the northern jet is much steeper than the southern jet, since at smaller separations the convolution with the beam across the core causes the intensity to be biased upwards.

ORCID iDs

Callan M. Wood https://orcid.org/0000-0002-2758-0864
James C. A. Miller-Jones https://orcid.org/0000-0003-3124-2814
Arash Bahramian https://orcid.org/0000-0003-2506-6041
Steven J. Tingay https://orcid.org/0000-0002-8195-7562
Steve Prabu https://orcid.org/0000-0003-3165-6785
Thomas D. Russell https://orcid.org/0000-0002-7930-2276
Pikky Atri https://orcid.org/0000-0001-8125-5619
Francesco Carotenuto https://orcid.org/0000-0002-0426-3276
Diego Altamirano https://orcid.org/0000-0002-3422-0074
Sara E. Motta https://orcid.org/0000-0002-6154-5843
Lucas Hyland https://orcid.org/0000-0002-4783-6679
Cormac Reynolds https://orcid.org/0000-0002-8978-0626
Dipankar Maitra https://orcid.org/0000-0003-1897-6872
Sera Markoff https://orcid.org/0000-0001-9564-0876
David M. Russell https://orcid.org/0000-0002-3500-631X
Craig L. Sarazin https://orcid.org/0000-0003-0167-0981
Gregory R. Sivakoff https://orcid.org/0000-0001-6682-916X
Roberto Soria https://orcid.org/0000-0002-4622-796X
Alexandra J. Tetarenko https://orcid.org/0000-0003-3906-4354
Valeriu Tudose https://orcid.org/0000-0001-5317-220X

References

Astropy Collaboration, Price-Whelan, A. M., Lim, P. L., et al. 2022, ApJ, 935, 167
Astropy Collaboration, Price-Whelan, A. M., Sipőcz, B. M., et al. 2018, AJ, 156, 123
Astropy Collaboration, Robitaille, T. P., Tollerud, E. J., et al. 2013, A&A, 558, A33
Baglio, M. C., Casella, P., Testa, V., et al. 2023, ATel, 16225, 1
Bahramian, A., Tremou, E., Tetarenko, A. J., et al. 2023, ApJL, 948, L7
Blandford, R. D., & Königl, A. 1979, ApJ, 232, 34
Bright, J., Farah, W., Fender, R., et al. 2023, ATel, 16228, 1
Bright, J. S., Fender, R. P., Motta, S. E., et al. 2020, NatAs, 4, 697
Carotenuto, F., Tetarenko, A. J., & Corbel, S. 2022, MNRAS, 511, 4826
Castro-Tirado, A. J., Sanchez-Ramirez, R., Caballero-Garcia, M. D., et al. 2023, ATel, 16208, 1
Chael, A. A., Johnson, M. D., Bouman, K. L., et al. 2018, ApJ, 857, 23
Charlot, P., Jacobs, C. S., Gordon, D., et al. 2020, A&A, 644, A159
Chaty, S., Dubus, G., & Raichoor, A. 2011, A&A, 529, A3
Corbel, S., Fender, R. P., Tzioumis, A. K., et al. 2000, A&A, 359, 251
Corbel, S., Fender, R. P., Tzioumis, A. K., et al. 2002, Sci, 298, 196
Corbel, S., Kaaret, P., Fender, R. P., et al. 2005, ApJ, 632, 504
Deller, A. T., Brisken, W. F., Phillips, C. J., et al. 2011, PASP, 123, 275
Deller, A. T., Tingay, S. J., Bailes, M., & West, C. 2007, PASP, 119, 318
Dhawan, V., Mirabel, I. F., & Rodríguez, L. F. 2000, ApJ, 543, 373
Dovciak, M., Ratheesh, A., Tennant, A., & Ma, G. 2023, ATel, 16242, 1
Echiburú-Trujillo, C., Tetarenko, A. J., Haggard, D., et al. 2024, ApJ, 962, 116
Espinasse, M., Corbel, S., Kaaret, P., et al. 2020, ApJL, 895, L31
Fender, R. P. 2001, MNRAS, 322, 31
Fender, R. P., Belloni, T. M., & Gallo, E. 2004, MNRAS, 355, 1105
Fender, R. P., Homan, J., & Belloni, T. M. 2009, MNRAS, 396, 1370
Foreman-Mackey, D. 2016, JOSS, 1, 24
Gandhi, P., Blain, A. W., Russell, D. M., et al. 2011, ApJL, 740, L13
Greisen, E. W. 2003, in Information Handling in Astronomy—Historical Vistas, ed. A. Heck (Dordrecht: Kluwer), 109
Harris, C. R., Millman, K. J., van der Walt, S. J., et al. 2020, Natur, 585, 357
Heinz, S. 2006, ApJ, 636, 316
Hjellming, R. M., & Rupen, M. P. 1995, Natur, 375, 464
Högbom, J. A. 1974, A&AS, 15, 417
Homan, J., Bright, J., Motta, S. E., et al. 2020, ApJL, 891, L29
Hunter, J. D. 2007, CSE, 9, 90
Ingram, A., Bollemeijer, N., Veledina, A., et al. 2023, ApJ, 968, 76
Jamil, O., Fender, R. P., & Kaiser, C. R. 2010, MNRAS, 401, 394
Kalamkar, M., Casella, P., Uttley, P., et al. 2016, MNRAS, 460, 3284
Kennea, J. A. & Swift Team 2023, GCN, 34540, 1
Kluyver, T., Ragan-Kelley, B., Pérez, F., et al. 2016, in Positioning and Power in Academic Publishing: Players, Agents and Agendas, ed. F. Loizides & B. Schmidt (Amsterdam: IOS Press), 87
Kravtsov, V., Nitindala, A. P., Veledina, A., et al. 2023, ATel, 16245, 1
Kreidberg, L., Bailyn, C. D., Farr, W. M., & Kalogera, V. 2012, ApJ, 757, 36
Malzac, J. 2014, MNRAS, 443, 299
Malzac, J., Kalamkar, M., Vincentelli, F., et al. 2018, MNRAS, 480, 2054
Markoff, S., Falcke, H., & Fender, R. 2001, A&A, 372, L25
Mata Sánchez, D., Muñoz-Darias, T., Armas Padilla, M., Casares, J., & Torres, M. A. P. 2024, A&A, 682, L1
Matsuoka, M., Kawasaki, K., Ueno, S., et al. 2009, PASJ, 61, 999
Migliori, G., Corbel, S., Tomsick, J. A., et al. 2017, MNRAS, 472, 141
Miller-Jones, J. C. A., Bahramian, A., Orosz, J. A., et al. 2021, Sci, 371, 1046
Miller-Jones, J. C. A., Blundell, K. M., & Duffy, P. 2004, ApJL, 603, L21
Miller-Jones, J. C. A., Jonker, P. G., Ratti, E. M., et al. 2011a, MNRAS, 415, 306
Miller-Jones, J. C. A., Sivakoff, G. R., Altamirano, D., et al. 2011b, in IAU Symp. 275, Jets at All Scales, ed. G. E. Romero, R. A. Sunyaev, & T. Belloni (Cambridge: Cambridge Univ. Press), 224
Miller-Jones, J. C. A., Sivakoff, G. R., Altamirano, D., et al. 2012, MNRAS, 421, 468

Miller-Jones, J. C. A., Sivakoff, G. R., Bahramian, A., & Russell, T. D. 2023, ATel, 16211, 1
Miller-Jones, J. C. A., Tetarenko, A. J., Sivakoff, G. R., et al. 2019, Natur, 569, 374
Mirabel, I. F., & Rodríguez, L. F. 1994, Natur, 371, 46
Mirabel, I. F., & Rodríguez, L. F. 1999, ARA&A, 37, 409
Nakajima, M., Negoro, H., Serino, M., et al. 2023, ATel, 16206, 1
Negoro, H., Serino, M., Nakajima, M., et al. 2023a, GCN, 34544, 1
Negoro, H., Serino, M., Nakajima, M., et al. 2023b, ATel, 16205, 1
O'Connor, B., Hare, J., Younes, G., et al. 2023a, GCN, 34549, 1
O'Connor, B., Hare, J., Younes, G., et al. 2023b, ATel, 16207, 1
Page, K. L., Dichiara, S., Gropp, J. D., et al. 2023, GCN, 34537, 1
Péault, M., Malzac, J., Coriat, M., et al. 2019, MNRAS, 482, 2447
Prabu, S., Miller-Jones, J. C. A., Bahramian, A., et al. 2023, MNRAS, 525, 4426
Pradel, N., Charlot, P., & Lestrade, J. F. 2006, A&A, 452, 1099
Reid, M. J., & Miller-Jones, J. C. A. 2023, ApJ, 959, 85
Reid, M. J., Menten, K. M., Zheng, X. W., et al. 2009, ApJ, 700, 137
Ribó, M., Dhawan, V., & Mirabel, I. F. 2004, in Proc. 7th. Symp. European VLBI Network on New Developments in VLBI Science and Technology, ed. R. Bachiller et al. (Madrid: Observatorio Astronomico Nacional of Spain), 111
Russell, T. D., Lucchini, M., Tetarenko, A. J., et al. 2020, MNRAS, 498, 5772
Russell, T. D., Miller-Jones, J. C. A., Curran, P. A., et al. 2015, MNRAS, 450, 1745
Russell, T. D., Soria, R., Miller-Jones, J. C. A., et al. 2014a, MNRAS, 439, 1390
Russell, T. D., Soria, R., Motch, C., et al. 2014b, MNRAS, 439, 1381
Russell, T. D., Tetarenko, A. J., Miller-Jones, J. C. A., et al. 2019, ApJ, 883, 198
Ryle, M. S., & Longair, M. S. 1967, MNRAS, 136, 123
Scheuer, P. A. G., & Readhead, A. C. S. 1979, Natur, 277, 182
Skilling, J. 2006, BayAn, 1, 833
Speagle, J. S. 2020, MNRAS, 493, 3132
Stirling, A. M., Spencer, R. E., de la Force, C. J., et al. 2001, MNRAS, 327, 1273
Tetarenko, A. J., Casella, P., Miller-Jones, J. C. A., et al. 2019, MNRAS, 484, 2987
Tetarenko, A. J., Casella, P., Miller-Jones, J. C. A., et al. 2021, MNRAS, 504, 3862
Tingay, S. J., Jauncey, D. L., Preston, R. A., et al. 1995, Natur, 374, 141
van der Velden, E. 2020, JOSS, 5, 2004
Veledina, A., Muleri, F., Dovčiak, M., et al. 2023, ApJL, 958, L16
Virtanen, P., Gommers, R., Oliphant, T. E., et al. 2020, NatMe, 17, 261
Vrtilek, S. D., Gurwell, M., McCollough, M., & Rao, R. 2023, ATel, 16230, 1
Wells, D. C. 1985, in Proc. 1st Workshop Data Analysis in Astronomy, ed. V. di Gesù et al. (New York: Plenum), 195
Wenger, M., Ochsenbein, F., Egret, D., et al. 2000, A&AS, 143, 9
Williams-Baldwin, D., Motta, S., Rhodes, L., et al. 2023, ATel, 16231, 1
Wood, C. M., Miller-Jones, J. C. A., Bahramian, A., et al. 2023, MNRAS, 522, 70
Wood, C. M., Miller-Jones, J. C. A., Homan, J., et al. 2021, MNRAS, 505, 3393
Woodburn, L., Natusch, T., Weston, S., et al. 2015, PASA, 32, e017
Yang, J., Brocksopp, C., Corbel, S., et al. 2010, MNRAS, 409, L64
Zdziarski, A. A., Veledina, A., Szanecki, M., et al. 2023, ApJL, 951, L45